M. Trisolini, C. Colombo, Y. Tsuda
Ejecta Models for Particles Generated by Small Kinetic Impactors onto Asteroid Surfaces
in: AIAA Scitech 2022 Forum, AIAA, 2022, ISBN: 9781624106316, p. 1-13, AIAA 2022-2383
[AIAA Scitech 2022 Forum, San Diego, CA, USA & Virtual Conference, 3-7 Jan. 2022]
doi:10.2514/6.2022-2383

Ejecta models for particles generated by small kinetic impactors onto asteroid surfaces

Mirko Trisolini *
Politecnico di Milano, Milan, Italy

Camilla Colombo †
Politecnico di Milano, Milan, Italy

Yuichi Tsuda ‡
Institute of Space and Astronautical Science (ISAS)/Japan Aerospace Exploration Agency (JAXA), Sagamihara, Japan

This work presents the development of a statistical ejecta model to predict the ejecta characteristics due to the impact of a small kinetic impactor onto asteroids surfaces. The distribution of the ejecta in terms of particle size, ejection velocity, and ejection direction is obtained. The procedure followed to compute the parameters defining the shape of the distribution is based on conservation law and comparison with experimental correlation. In the context of the CRADLE project, the developed model is used to estimate the number of collectable particles as a function of the target characteristics.

I. Introduction

Space exploration missions to asteroids have always drawn the attention of the scientific and engineering community given the challenges they pose and the possibility they present to further our knowledge of the Solar System. Asteroids carry fundamental information on the evolution of our Solar System. They are rich in valuable resources such as metals, silicates, and water, which could be exploited through future asteroid mining missions, and enable long-duration mission self-sustaining. The physical composition of asteroids is varied and, in most cases, poorly understood; it can be significantly improved collecting and studying their samples. Improving our knowledge, we can better target asteroids to be exploited for future material extraction and increase the efficiency of asteroid deflection missions. Several missions have visited asteroids and other small bodies; however, only few have orbited, landed, or impacted on them. Examples are JAXA missions Hayabusa and Hayabusa2 [1–3], ESA Rosetta, and NASA OSIRIS-REx.

In a context of future asteroid exploration missions, within the CRADLE project (Collecting Asteroid-Orbiting Samples) [4, 5] funded by the Marie Curie Action (MSCA) (Grant Number 896404), we envision the possibility to perform in-orbit collection as an alternative to landing or touchdown operations. Such a collection mechanism is based on the knowledge of the dynamical behaviour of the small particles orbiting the asteroid, which can be generated by means of a small kinetic impactor mission. Given that the dynamical evolution of such particles is influenced by their size and ejection velocity, it is important to understand the influence of the ejecta models used to generate the initial conditions after the impact.

In this work, we present the development of a distribution-based ejecta model, describing the particle density as a function of the size, ejection speed and ejection direction (both in-plane and out-of-plane components). Finally, we apply this model to estimate the number of collectable particles after a small kinetic impact onto an asteroid, studying the different outcomes as a function of the asteroid characteristics, i.e., size, density, material and strength.

II. Ejecta model

The objective of this section is to describe the advancements in the development of a distribution-based ejecta model, describing the ejection conditions of particles created by a small kinetic impactor. The development of this model fits within the larger picture of the CRADLE project as a step towards the modelling and analysis of the particles' evolution around the asteroids in terms of densities and fluxes. In fact, it is possible to describe the motion of a large number of

*mirko.trisolini@polimi.it, MSCA Research Fellow, Department of Aerospace Science and Technology, via La Masa 34, 20156, Milan, Italy.
†camilla.colombo@polimi.it, Associate Professor, Department of Aerospace Science and Technology, via La Masa 34, 20156, Milan, Italy.
‡tsuda.yuichi@jaxa.jp, Professor/Hayabusa2 Project Manager.

small particles under the dynamical influence of the asteroid and the Sun as a continuum [7] and directly predict the evolution of their density in space and time. To do so, we also need a continuum description of the ejection conditions as a function of the state variables: particle size, ejection speed, and launch direction. Once the density distribution function of the particles condition at ejection is obtained, we can used as initial condition for the continuum propagation, thus predicting the evolution of the ensemble of particles as a whole. This work, focuses on the development of such particle ejection models. We first consider the distribution in size and speed Section II.A and then we add the contribution of the launch direction Section II.B.

A. Size and speed distribution

For the distribution in size and speed, we base our model on the work of Sachse [8], extending it to the application for small kinetic impactor onto small bodies, and in particular asteroids. We consider two types of distributions, with expression of the form:

$$f_u(s,u) = As^{-1-\bar{\alpha}}u^{-1-\bar{\gamma}} \tag{1}$$

$$f_c(s,u) = As^{-1-\bar{\alpha}}u^{-1-\bar{\gamma}} \cdot \Theta\left[bs^{-\bar{\beta}} - u\right] \tag{2}$$

where s is the particle radius, u the particle velocity, Θ is the Heaviside step function, and A, b, $\bar{\alpha}$, $\bar{\beta}$, and $\bar{\gamma}$ are parameters that characterise the shape of the distribution function. The first expression, f_u, represents an uncorrelated distribution that is a distribution in which the size and speed of the particles is not mutually dependent. This is a typical approximation for ejecta models [9]. The second expression, f_c, is instead a correlated distribution in which the particle speed depends on the particle size. Specifically, the larger the particle, the smaller the velocity is, on average.

1. Uncorrelated distribution

In order to fully define the distribution we need to compute the unknown coefficient. We specialise the computation of the coefficients for the case of impact on small bodies, exploiting experimental correlations [10–12] and conservation laws. As Eq. (1) can be expressed as $f_u(s,u) = g(s)h(u)$, with a combination of a distribution function in s and one in u, we can treat the two expressions separately. Following the work of Krivov [7], we first focus on the size distribution, expressing the cumulative distribution function as a power low.

$$G(s > S) = N_r \cdot s^{-\bar{\alpha}} \tag{3}$$

where N_r can be determined from the mass conservation law and $\bar{\alpha}$ is a coefficient defining the slope of the power law. Table 1 shows some examples of possible values for the $\bar{\alpha}$ coefficient [8].

Table 1 Examples of $\bar{\alpha}$ coefficients for different types of targets.

Target	Range
Icy target	[1.2, 2.5]
Basalt	[2.4, 2.7]
Regolith	~ 2.25

Differentiating Eq. (3), we obtain the density distribution function, which has the following expression:

$$g(s) = \bar{\alpha}N_r s^{-1-\bar{\alpha}} \tag{4}$$

we can then obtain N_r from mass conservation as follows:

$$M_{\text{tot}} = \frac{4}{3}\pi\rho \int_{s_{\min}}^{s_{\max}} s^3 g(s) ds \quad \rightarrow \quad N_r = \frac{3(3-\bar{\alpha})M_{\text{tot}}}{4\bar{\alpha}\left(s_{\max}^{3-\bar{\alpha}} - s_{\min}^{3-\bar{\alpha}}\right)\pi\rho} \tag{5}$$

where M_{tot} is the total mass ejected from the crater, ρ is the density of the asteroid, and $s_{\min}$ and $s_{\max}$ are the minimum and maximum particle radii, respectively. The minimum and maximum radii are a free parameter that can be

selected by the user. Commonly selected values are 10-100 μm for the minimum diameter and 10 cm for the maximum one. The total mass can be computed from experimentally derived correlations as follows [10]:

$$M_{\rm tot} = k\rho\left((n_2 R)^3 - (n_1 a)^3\right) \tag{6}$$

where k, n_1, and n_2 are coefficients depending on the type of material and impact derived from experimental correlations. The works of Housen and Holsapple contain extensive coverage for the derivation and usage of these parameters. The interested reader is referred to their work [10–12]. Finally, R is the crater radius and a is the impactor diameter.

We can proceed in a similar fashion for the velocity distribution, $h(u)$. Assuming the distribution is of the form $h(u) = C \cdot u^{-1-\bar{\gamma}}$. To compute the constant C, we simply impose that the integral of the probability density function is equal to unity, as follows:

$$\int_{u_{\rm min}}^{u_{\rm max}} h(u)du = 1 \quad \rightarrow \quad C = \frac{\bar{\gamma}}{u_{\rm min}^{-\bar{\gamma}} - u_{\rm max}^{-\bar{\gamma}}} \tag{7}$$

Finally, we have the following expression for the uncorrelated distribution:

$$f_u(s,u) = \bar{\alpha} C N_r s^{1-\bar{\alpha}} u^{1-\bar{\gamma}} \quad \text{with } s_{\rm min} \leq s_{\rm max} \text{ and } u_{\rm min} \leq u_{\rm max} \tag{8}$$

In Eqs. (2) and (7), the values of the minimum and maximum ejection speeds can be provided by the user. Possible values can be derived from the experimental correlation of ejection speed as function of the launch position (Eq. (9) [10]), evaluated at the extreme of the crater ($u_{\rm min} = u(x_{\rm max}) = u(n_2 R)$, $u_{\rm max} = u(x_{\rm min}) = u(n_1 a)$):

$$\frac{u}{U} = C_1\left[\frac{x}{a}\left(\frac{\rho}{\delta}\right)^{\nu}\right]^{-1/\mu} \tag{9}$$

where U is the impactor speed, x the distance from the centre of the crater, δ the projectile density, and ν a material-dependent coefficient [10].

The only thing left is to determine the value of the exponent $\bar{\gamma}$. This can be obtained checking how the cumulative distribution of the mass as function of the ejection speed (Eq. (10)) scales and comparing it with experimental correlations obtained by Housen [10] ($M(<u) \propto u^{-3\mu}$).

$$M(<u) = \int_{u_{\rm min}}^{u}\left[\frac{4}{3}\pi\rho h(u)\cdot\int_{s_{\rm min}}^{s_{\rm max}} s^3 g(s)ds\right]du = \int_{u_{\rm min}}^{u} M_{\rm tot} h(u)du = \frac{C}{\bar{\gamma}}\left(u_{\rm min}^{-\bar{\gamma}} - u^{-\bar{\gamma}}\right)M_{\rm tot} \tag{10}$$

From the comparison, we have $\bar{\gamma} = 3 \cdot \mu$, where μ depends on the material considered.

2. Correlated distribution

The correlated distribution of Eq. (2) has two additional parameters with respect to the uncorrelated one, specifically, b and $\bar{\beta}$. The computation of the parameters is thus more complex, also given the different codependencies between the parameters. For the correlated distribution we follow the approach of Sachse [8], which introduces three additional coefficients (α, β, γ) with the following meaning:

$$g(s) = \int_{u_{\rm min}}^{u_{\rm max}} f_c(s,u)du \;\sim\; s^{-1-\alpha} \tag{11}$$

$$\bar{u}(s) = \frac{1}{g(s)}\int_{u_{\rm min}}^{u_{\rm max}} u f_c(s,u)du \;\sim\; s^{-\beta} \tag{12}$$

$$m(u) = \frac{4}{3}\pi\rho\int_{s_{\rm min}}^{s_{\rm max}} s^3 f_c(s,u)ds \;\sim\; u^{-1-\gamma} \tag{13}$$

Therefore, α regulates the amount of particles, β the slope of the size-averaged ejection speed, and γ the amount of ejected mass as a function of the speed. The parameter α depends on the target material and ranges from 1.5 for looses to 3 for solid targets, β is always grater than zero and, usually smaller than 1, while γ depends on the target material and ranges between 1 for porous to 2 for non-porous materials [8]. Sachse also shows that α, β and γ are related to $\bar{\alpha}$, $\bar{\beta}$ and $\bar{\gamma}$ as follows:

$$\bar{\alpha} = \alpha \tag{14}$$

$$\bar{\beta} = \frac{3 - \alpha - \beta}{\gamma - 1} \tag{15}$$

$$\bar{\gamma} = \gamma + \frac{\alpha - 3}{\bar{\beta}} \tag{16}$$

Given the limits in α, β and γ, we also have range limitations for $\bar{\alpha}$, $\bar{\beta}$ and $\bar{\gamma}$ that need to be taken into account. Specifically, $0 < \bar{\alpha} < 3$ and $0 < \bar{\gamma} < 1$ [8]. In addition, Sachse already derived the expressions for the particle density and ejected mass, which are the following:

$$g(s) = \frac{A}{\bar{\gamma}} s^{-1-\bar{\alpha}} \left(u_{\min}^{-\bar{\gamma}} - b^{-\bar{\gamma}} s^{\bar{\beta}\bar{\gamma}} \right) \tag{17}$$

$$m(u) = \frac{4}{3}\pi\rho \frac{A}{\bar{\alpha} - 3} u^{-1-\bar{\gamma}} \left(s_{\min}^{3-\bar{\alpha}} - b^{-\frac{\bar{\alpha}-3}{\bar{\beta}}} u^{\frac{\bar{\alpha}-3}{\bar{\beta}}} \right) \tag{18}$$

In general, to use Eqs. (2), (17) and (18) to define the ejecta distribution in size and speed, we can start be defining a value for the maximum ejection speed and the minimum particle size. Both these quantities can be reasonably assumed or computed. In the first case, for the maximum ejection speed, we can refer to experimental correlations, such as Eq. (9), while in the second case, for the minimum size, this can be reasonably assumed (10-100 µm) or assumed equal to the minimum size detectable by an instrument [8]. Once these values are given, we select a value for $\alpha = \bar{\alpha}$ and $\gamma = 3\mu$, which only depend on the material type. At this point, we are only missing three parameters, A, β, and b; however, they must be selected carefully as they must also satisfy the mass conservation equation. In addition, b is related to $\bar{\beta}$ by the Heaviside function because the Heaviside function returns one only if its argument is greater than zero. Practically, this expression limits the maximum ejection speed as a function of the particle size. Fig. 1 shows the density distribution of the ejection speed for different particle sizes and for the two extreme values of the free parameter β. We can clearly see from Fig. 1 the cutting effect of the Heaviside function and that the cut-off velocity is smaller the greater is the particle size. In addition, we see that a larger β returns a narrower and less steep distribution.

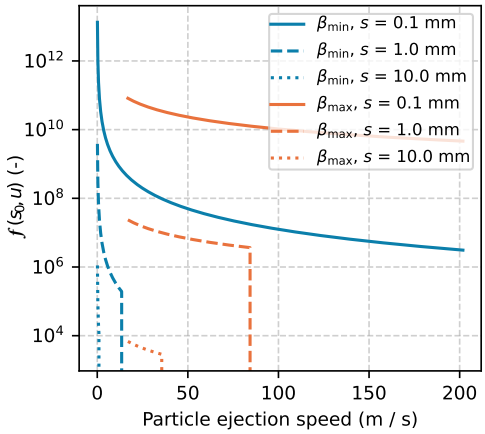

Fig. 1 Ejection speed density distribution as function of particle size and β parameter.

Following Sachse's procedure we can thus write:

$$b = u \cdot s^{\bar{\beta}} \tag{19}$$

As Eq. (19) gives us a relation between b and $\bar{\beta}$, if we define $\bar{\beta}$, our ejecta model is completely defined. Now, $\bar{\beta}$ is a function of α, β, and γ. We already know how to obtain α and γ; therefore, we are only missing β. However, as previously mentioned, β cannot be picked freely for two reasons: first, the limitation in ranges of α and γ impose limits

also on β; second, the mass conservation must be satisfied. Given the values of α and γ, the previously mentioned limitation in $\bar{\gamma}$, and the fact that β must be grater than zero, we can identify the following range: $0 < \beta < \beta_{\max}$, where:

$$\beta_{\max} = (3 - \alpha) \cdot \left(1 - \frac{\gamma - 1}{\gamma}\right) \tag{20}$$

At this point, we must satisfy the mass conservation equation as follows:

$$M_{\text{tot}} = \frac{4}{3}\pi\rho \int_{s_{\min}}^{s_{\max}} s^3 g(s) ds = \int_{u_{\min}}^{u_{\max}} m(u) du \tag{21}$$

where $g(s)$ is the expression of Eq. (17), $m(u)$ is computed with Eq. (18), and M_{tot} is again computed using Eq. (6). By selecting a value of β between 0 and $\beta_{\max}$ we derive the corresponding value of b using Eq. (19). Then, we solve both equations Eq. (21) to obtain the corresponding values of A and $u_{\min}$, which satisfy the mass conservation law. After this procedure, the correlated distribution is defined and is a function of a "free" parameter β. Fig. 2 shows an example of the effects of changing the free parameter β. We can clearly see that the parameter β regulates the velocity distribution of the particles, also as a function of their size; specifically, larger values of β lead to larger average speeds and a more "linear" (in log-log space) behaviour of the average speed as a function of the particle size (plot on the right). This in turn influences the cumulative ejected mass as a function of the speed, with most of the mass ejected at low velocities for lower values of β.

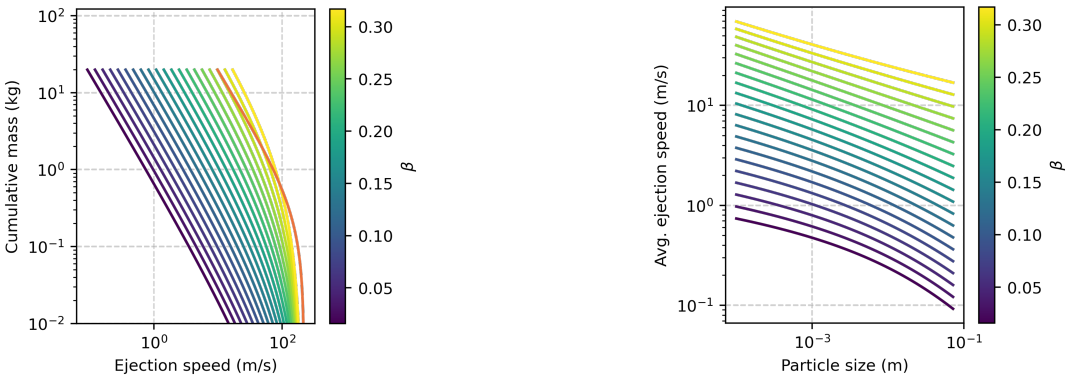

Fig. 2 Example of the effects of β. Left: Cumulative ejection mass vs particle speed. Right: Mean ejection speed vs. particle size.

Despite β is a free parameter, we can try to select it exploiting the knowledge derived from experimental correlations. Specifically, we can again leverage the work of Housen and Holsapple [10–12] to get the minimum ejecta velocity for a given impact (Eq. (9)). Using this value of $u_{\min}$ we can compute the corresponding value of β. An example of the characteristics of such a distribution is given in Fig. 3, where we show the cumulative mass distribution as function of the ejection speed. In red, the difference between the two experimentally derived expressions by Housen [10], one considering the material porosity (solid line) and the other without (dashed line). The derivation of the distribution developed in this work are based on the experimental correlation without porosity that is the expressions for the minimum and maximum ejection speeds were derived from this correlation. In fact, it is possible to observe that the cumulative distribution derived from the uncorrelated case (blue line) closely matches this experimental correlation. The correlated case, instead, shows a steeper behaviour that is coherent with the limitations on the maximum velocity vs particle size.

Fig. 4 shows an example of the two distributions of Eqs. (1) and (2) for the same impact in log-log scale. We can see the clear difference between the two cases, particularly the "cut-off" portion of the distribution due to the Heaviside function, which does not allow larger particles to have high speeds. In addition, we see how the correlated distribution has on average higher speeds for lower diameters, as it is also confirmed by Fig. 5.

B. Launch direction distribution

To fully characterise the output of an impact event, alongside the distribution in size and speed, we also need the distribution of the ejection direction. In this work, we only consider normal impacts and we identify the ejecta launch direction with two angles: an in-plane launch angle, θ, and an out-of-plane ejection angle, ψ. As we are considering

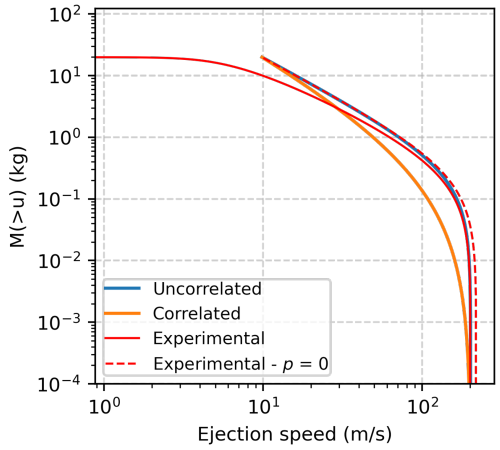

Fig. 3 Comparison of cumulative ejection mass vs particle speed.

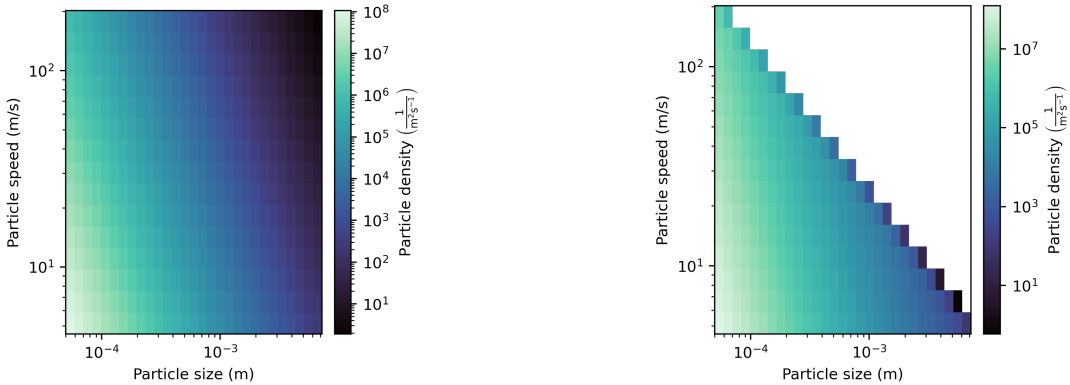

Fig. 4 Comparison of 2D size vs ejection speed density distributions. Left: Uncorrelated case. Right: Correlated case.

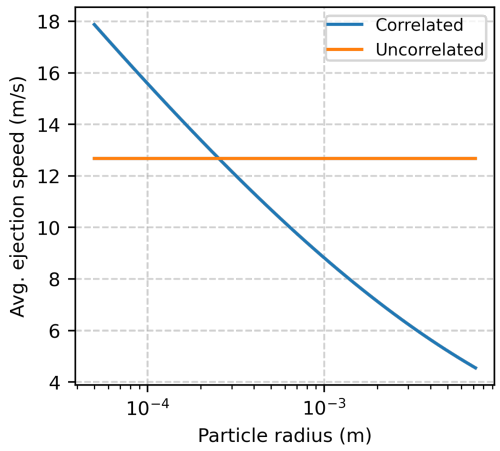

Fig. 5 Comparison between the mean ejection speed for correlated and uncorrelated distributions.

normal impacts, and neglecting the uneven structure of the terrain, we can assume the distribution in θ to be uniformly distributed over 2π that is

$$f_\theta(\theta) = \frac{1}{2\pi} \quad \text{with } 0 \leq \theta \leq 2\pi \tag{22}$$

For the out-of-plane ejection angle ψ, we can consider two types of distribution. A spherically uniform distribution within a minimum and maximum value of ψ (a spherical sector), or a distribution that is a combination of Gaussians as proposed by Richardson [13].

1. Uniform distribution

In case of a uniform distribution over a spherical sector delimited by a minimum ($\psi_{\min}$) and a maximum ($\psi_{\max}$) ejection angle, we can express the probability density function as follows:

$$f_\psi(\psi) = \frac{\cos\psi}{\sin\psi_{\max} - \sin\psi_{\min}} \quad \text{with } \psi_{\min} \leq \psi \leq \psi_{\max} \tag{23}$$

where the denominator is used to normalise the distribution.

2. Gaussian mixture distribution

To have an out-of-plane launch angle distribution that is not uniform with the ejection angle, we can use the experimentally derived expression of Richardson [13]. In his work, Richardson derives from experimental results that the ejection angle distribution can be approximated as follows:

$$\psi(r) = \psi_0 - \psi_d \cdot \left(\frac{r}{R}\right) \tag{24}$$

where $\psi_0 = 52.4^\circ \pm 6.1^\circ$ and $\psi_d = 18.4^\circ \pm 8.2^\circ$ with 2σ errors. Starting from this expression, we can transform it into a distribution assuming that ψ_0 and ψ_d can be represented with Gaussian distributions: $\psi_0 = \mathcal{N}_0(\mu_0, \sigma_0)$ and $\psi_d = \mathcal{N}_d(\mu_d, \sigma_d)$, where $\mu_0 = 52.4$, $\mu_d = 18.4$, $\sigma_0 = 3.05$, and $\sigma_d = 4.1$. Before obtaining the distribution in the out-of-plane ejection angle, we need to consider its dependency from the ejection position, r. At the moment, we are trying to maintain the ejection distribution uncorrelated from the size and velocity distributions, to avoid unnecessary complications. AS the ejection location, r, is directly connected to the ejection speed, u, we first want to eliminate it from Eq. (24). To do so, we average out the contribution over the crater radius as follows:

$$f_\psi(\psi) = \mathcal{N}_0(\mu_0, \sigma_0) + \frac{1}{R} \cdot \int_0^R \mathcal{N}_d(-\mu_d, \sigma_d)\left(\frac{r}{R}\right) dr = \mathcal{N}_0(\mu_0, \sigma_0) + \frac{1}{2}\mathcal{N}_d(-\mu_d, \sigma_d) = \mathcal{N}_n(\mu_n, \sigma_n) \tag{25}$$

where $\mu_n = \mu_0 - \frac{\mu_d}{2}$ and $\sigma_n^2 = \sigma_0^2 + \left(\frac{\sigma_d}{2}\right)^2$. Therefore for the distribution in ψ, we have:

$$f_\psi(\psi) = \frac{1}{\sigma_n\sqrt{2\pi}} \exp\left\{\left[-\frac{1}{2}\left(\frac{\psi - \mu_n}{\sigma_n}\right)\right]\right\} \tag{26}$$

Combining the contributions of Section II.A and Section II.B we can obtain the full distribution description of the ejection conditions.

III. Collection strategy and target selection

As mentioned in Section I, the CRADLE project aims at studying alternative to sample collection missions that leverage the dynamical behaviour of the particles around small bodies after a kinetic impact, to try to collect the samples while in-orbit, thus avoiding landing or touchdown. Given the peculiarities of the ejecta behaviour after an hypervelocity impact, we want to study if the characteristics of the target, an asteroid in this case, can affect the possibility of collecting the samples. In fact, to perform a collection we need the samples to orbit the asteroid for a sufficient time after the impact so that the spacecraft has enough time to collect the particles. As we can expect, the dynamics of the particle around an asteroid and in particular its residence time, varies as a function of the perturbations it receive from the environment. Therefore, it is a function of the distance from the Sun, the size and shape of the asteroid, and the material of the asteroid. In addition, the dynamical behaviour its influenced by the initial conditions that is the impact event, which can be modelled as described in Section II. Therefore, in this work, we seek to analyse the effects of the target characteristics on the in-orbit sample collection by combining the dynamical evolution of the samples and the modelling of the ejection event. By following this approach, a complete understanding of the collection capabilities can be obtained.

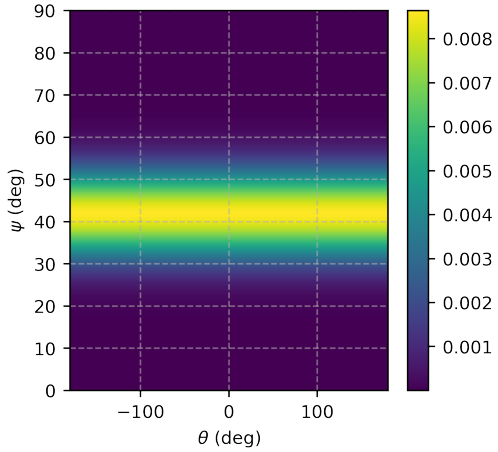

Fig. 6 2D launch direction distribution in θ and ψ.

A. Dynamical model

The adopted dynamical model is the Circular Restricted Three-Body Problem (CR3BP) perturbed by Solar Radiation Pressure (SRP) [14]. The equations of motion are expressed in non-dimensional form in a synodic reference frame centred in the asteroid.

$$\begin{cases} \ddot{x} - 2\bar{n}\dot{y} = V_{/x} \\ \ddot{y} + 2\bar{n}\dot{x} = V_{/y} \\ \ddot{z} = V_{/z} \end{cases} \tag{27}$$

where x, y, and z are the non-dimensional particle positions with respect to the centre of the asteroid in the rotating frame, and $\bar{n}$ is the non-dimensional mean motion, equal to unity in this case. The potential V is expressed as follows:

$$V = \frac{1}{2}\left(x^2 + y^2\right) + (1-\mu)\,x + \frac{(1-\beta)\,(1-\mu)}{r_{\mathrm{sp}}} + \frac{\mu}{r_{\mathrm{ap}}} + \frac{1}{2}\,(1-\mu)^2 \tag{28}$$

with $\mu = \frac{\mu_a}{\mu_a+\mu_s}$, r_{sp} and r_{ap} the distances between the Sun and the particle and the asteroid and the particle, respectively. The lightness parameter β can be expressed as follows:

$$\beta = \frac{P_0}{c}\frac{AU^2}{\mu_{Sub}}\frac{3c_{\mathrm{R}}}{2\rho_{\mathrm{p}}d_{\mathrm{p}}} \tag{29}$$

Where $P_0 = 1367\ \mathrm{W/m^2}$ is the solar flux at 1 AU, c is the speed of light, AU is the astronomical unit, ρ_{p} is the particle density and d_{p} the particle diameter.

B. Collection evaluation

The collection strategy analysed in this work aims at collecting the particles that will orbit the asteroid for enough time (to be defined based on operational constraints) [4]. Therefore the main criteria to consider is the number of particles still orbiting the asteroid after a predefined amount of time: we consider collectable all those particles that orbit the asteroid for enough time before re-impacting the asteroid surface.

To understand the feasibility and quality of the collection we estimate the number of collectable particles. We follow the approach described in the following. We first specify a particle range of interest for collection. In this case we consider the range between 0.1 and 3 mm. Then we select a range of ejection velocities to consider. We can, for example, estimate this range assuming a Keplerian motion and fixing a minimum and maximum collection period. Then we propagate the trajectories as in Section III.A, performing a grid analysis for both the ejection location on the asteroid's surface and the launch angles. For this analysis we limit our study to a 2D problem; therefore, we have a grid in ejection location every 45° and a grid in launch angle every 5°, uniformly distributed between 25° and 65°. We then identify the percentage of particles still orbiting the asteroid for a time greater than a specified threshold (6 hours

in this case). Finally, we estimate the number of particles still in orbit by combining the dynamical behaviour with the distribution of Section II.A. In fact, to estimate the number of particles, we integrate the ejecta distribution in the selected size and speed ranges and we weight this distribution with the previously computed percentage of particles still orbiting. In this way, we obtain the following Figure of Merit (FOM):

$$\mathrm{FOM} = \log_{10}\left[\sum_{k=0}^{n_d}\left(\int_{s_k}^{s_{k+1}}\int_{u_{\min}}^{u_{\max}} w_k f(s,u)\,ds\,du\right)\right] \tag{30}$$

where n_d is the number of bins in which we divide the particle diameter range and w_k is the weight representing the percentage of particles still orbiting. As the diameter influences the dynamical behaviour, different fractions of particles will still be orbiting as a function of their dimensions. Therefore, each contribution is weighted differently.

In this work, we present the results obtained following the aforementioned procedure. As the main objective of the paper is to address the feasibility of in-orbit collection for specific targets, we combine the effects of realistic impact conditions, modelled as described in Section II, with the dynamics of small particles perturbed by SRP. It is important at this point to remember that the composition of most asteroids is still unknown, leading to a considerable uncertainty when it comes to predicting their density and soil strength. As these parameters have a strong influence on the outcome of the ejecta model, it is critical to perform a parametric analysis considering different material types and strength levels. In the following, we consider three different types of materials commonly used for modelling asteroid's soil [9, 10, 13] and we apply the developed ejecta model to them. The considered materials are *sand*, *Weakly Cemented Basalt* (WCB), and *Sand anf Fly Ashes* (SFA). The first material is representative of very loose soil with strength close to zero: therefore, they are used to model gravity-dominated impacts. The second material is representative of weakly cohesive soils, similar to regolith [12]. The material properties relative to the ejecta model formulation are summarised in Table 2.

Table 2 Ejecta model material properties.

	Sand	WCB	SFA
μ	0.41	0.46	0.4
C_1	0.55	0.18	0.55
k	0.3	0.3	0.3
n_1	1.2	1.2	1.2
n_2	1.3	1	1
Y (MPa)	0	0.45	4×10^{-3}
α (Eqs. (1) and (2))	2	2.7	2.4

The analysis considers a range of possible asteroid sizes and densities. Specifically, the radius of the asteroid varies from 100 m to 15 km, while the asteroid density from 1 g cm^{-3} to g cm^{-3}. The radius range derives from data in the NASA asteroid small body database, excluding small objects. The density ranges are derived from average densities of common asteroid spectral classes [15].

Fig. 7 shows the results of the computation of the FOM for the three different materials. The sand-like material is considered to have zero strength, while the WCB and SFA are considered to have very low strength for this comparison. We can observe a similar behaviour between the materials, but with some differences. The first feature we can observe is the presence of an infeasibility region only for the WCB and SFA materials. In fact, all combinations of radius and density lead to possible collections in case of a sand-like material. This is a consequence of the relation between the minimum ejection velocity and the strength of the material: the higher the strength the greater is the minimum ejection speed (Eq. (9)). Therefore, for smaller and less dense asteroids for which the escape velocity is small, the particles cannot stay trapped around the asteroid for a sufficient time to be collected. However, this behaviour also causes the second notable feature of the plots. In fact, it is possible to observe in the centre and right plots that the highest FOM is concentrated close to the border with the infeasible region. This is a consequence of the fact that the ejecta distribution has its peak close to the minimum velocity (Fig. 4). Therefore, if the required ejection speed is close to the minimum one, a higher number of particles will be available for collection.

Maps similar to the ones of Fig. 7 have been obtained for the three material and different ranges of strength. We then used these maps to estimate the number of collectable particles for asteroids in the database, by locating them on

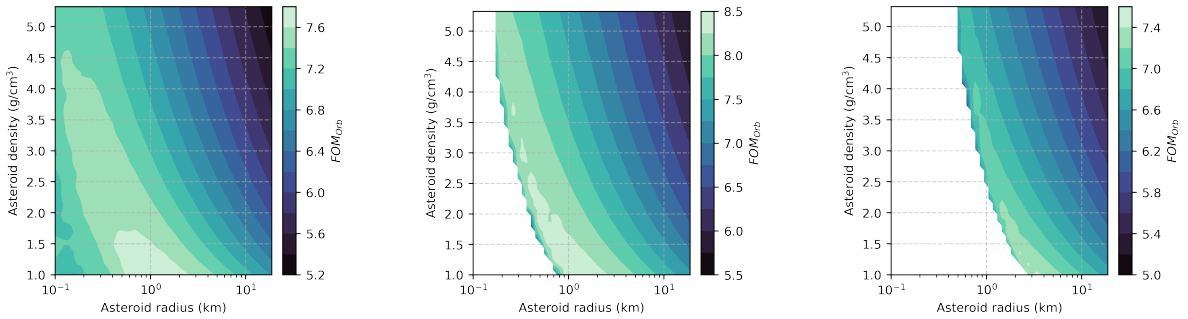

Fig. 7 FOM as function of the target size and density for three materials. Left: Sand-like material (Y = 0 Pa). Centre: WCB (Y = 1 kPa). Right: SFA (Y = 1 kPa)

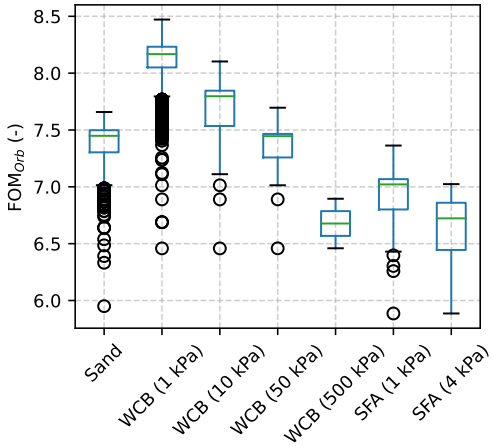

Fig. 8 Boxplot of the FOM as function of the material type and strength.

the maps given their size and density. In case the size was not available, it has been estimated from the albedo and magnitude information*. Similarly, for the density, when not available, it has been estimated from the spectral class of the asteroid [15]. Fig. 8 shows a summary of the obtained Figure of Merit for seven combinations of material type and strength. We can observe that low-strength WCB generates the highest amount of collectable particles, while a sand-like material, despite not having infeasibility regions, generates less particles (comparable to a mid-strength WCB). Sand and fly ashes, instead, are comparable to high strength WCB; in addition, they have a large infeasibility region for comparable strength values.

Finally, Fig. 9 shows the computation of the FOM for the asteroid database, also including an estimate of the Δv required to reach them. We can observe again that the number of available targets is proportional to the strength of the material, we high-strength WCB giving only two possible targets. We can also observe that several targets are feasible for low to mid-strength material types, and they also have competitive costs in terms of Δv, with a high percentage of options below 10 km s^{-1}.

Table 3 shows the top ten ranked asteroids in terms of Figure of Merit for each of the considered combination of material type and strength (excluding the highest WCB strength of 500 kPa). In the table, the potential target asteroid are ordered based on the required Δv in ascending order. It is interesting to observe how the possible *best targets* change as a function of the material type and strength. It should also be noted that we are showing only the top ten for each case but other targets will be available for each case. For example, in for the Sand case, several other targets in the list are possible, however they are outside the top ten best in terms of FOM index, and their value is not shown. It is also interesting to observe that the 10 kPa WCB case has a very similar behaviour to the 1 kPa SFA case. Table 3 is an valuable reference for the target selection of possible in-orbit particle collection missions as a function of the expected material of the target asteroid, which can sometimes be inferred based on the spectral class of the asteroid and with a

*https://cneos.jpl.nasa.gov/tools/ast_size_est.html

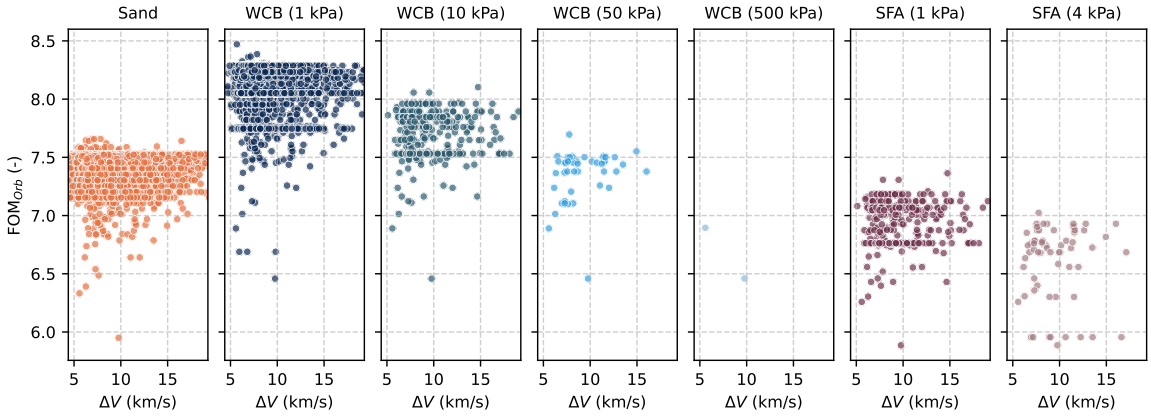

Fig. 9 Target selection trade-off for the orbiting collection strategy.

more refined observation campaign. It is also useful to select those asteroids which present "more robust" solutions for the collection that is the one with a collectability in most of the material type and strength combinations (e.g., Eros and Anteros).

IV. Conclusions and Discussion

In this work, the development of a distribution-based ejecta model is presented. The model and its coefficients are derived from experimental correlations and conservation laws. We show how the model can be defined and the coefficients determined. Particularly we present the difference between a correlated and an uncorrelated distribution in size and velocity and we show the sensitivity of the correlated distribution to the selection of the parameters defining the distribution. The effect of the free parameter β can be tuned in order to align the distribution with experimentally derived correlations.

In the second part of the work, we present a preliminary analysis of the collection feasibility for in-orbit particle collection missions as studied in the CRADLE project. Specifically we analyse a collection scenario in which we want the particle to orbit the asteroid for a sufficient amount of time in order to enable the collection by the spacecraft. The analysis leverage the characteristics of the developed ejecta model as it is used to estimate the number of collectable particles given the range of particle sizes and velocities that lead to a satisfying collection scenario. Feasibility regions have been identified considering relevant characteristics of the target (i.e., the asteroid radius and density). The analyses have been performed also considering uncertain parameters such as the material type and the material strength of the asteroid. Specifically, sand-like, WCB, and SFA materials have been considered. From the results, the orbiting collection option seems favoured by sand-like materials as no infeasible regions can be identified. A Figure of Merit (FOM) has been developed for a preliminary assessment of the collection capabilities as function of the target properties. In fact, the FOM is directly related to an estimate of the collectable particles. The results shows that the collection option can be more efficient for smaller asteroids. Finally, the FOM has been used to rank possible target asteroids and a shortlist of possible candidate is given, considering also the variability of the target material and strength.

Funding Sources

This project has received funding from the European Union's Horizon 2020 research and innovation programme under the Marie Sklodowska-Curie grant agreement No 896404 – CRADLE.

References

[1] Tsuda, Y., Yoshikawa, M., Abe, M., Minamino, H., and Nakazawa, S., "System design of the Hayabusa 2—Asteroid sample return mission to 1999 JU3," *Acta Astronautica*, Vol. 91, 2013, pp. 356–362.

[2] Tsuda, Y., Yoshikawa, M., Saiki, T., Nakazawa, S., and Watanabe, S.-i., "Hayabusa2–Sample return and kinetic impact mission to near-earth asteroid Ryugu," *Acta Astronautica*, Vol. 156, 2019, pp. 387–393.

Table 3 Asteroid ranking.

Asteroid	Sand	WCB (1 kPa)	WCB (10 kPa)	WCB (50 kPa)	SFA (1 kPa)	SFA (4 kPa)	Δv (km s^{-1})
Ryugu	7.29	-	-	-	-	-	4.39
Itokawa	7.21	-	-	-	-	-	4.61
Bennu	7.24	-	-	-	-	-	4.8
Nereus	7.35	-	-	-	-	-	4.97
Anteros	7.25	7.93	7.86	-	7.08	-	5.11
Orpheus	7.30	-	-	-	-	-	5.50
Norwan	7.37	8.07	-	-	-	-	5.50
Huma	**7.52**	**8.05**	-	-	-	-	5.52
Anagolay	7.50		-	-	-	-	5.53
Eros	-	6.89	6.89	6.89	6.25	6.25	5.58
Akka	-	8.18	-	-	-	-	5.65
Nyx	-	**8.47**	-	-	-	-	5.68
Lucianotesi	-	7.90	-	-	-	-	5.70
Belenus	-	8.19	-	-	-	-	5.77
Vinciguerra	-	8.29	-	-	-	-	5.82
Zephyr	-	-	7.65	-	6.87	-	5.86
Geographos	-	-	7.93	-	7.15	-	6.08
Ivar	-	-	7.23	7.24	6.56	6.56	6.15
McAuliffe	-	-	7.86	-	7.09	-	6.18
Seleucus	-	-	7.62	-	**8.86**	-	6.20
Oze	-	-	7.37	7.36	6.65	6.63	6.33
Ptah	-	-	7.85	-	7.07	-	6.37
Toro	-	-	7.73	-	6.98	-	6.43
Toutatis	-	-	-	**7.51**	-	6.85	6.50
Pygmalion	-	-	-	-	-	5.95	6.96
Alinda	-	-	-	7.10	-	6.76	6.96
Eric	-	-	-	7.12	-	6.46	7.29
Cleobulus	-	-	-	-	-	6.35	7.30
Cuno	-	-	-	7.45	-	**6.78**	7.32
Zeus	-	-	-	7.50	-	-	7.60

[3] Tsuda, Y., Saiki, T., Terui, F., Nakazawa, S., Yoshikawa, M., Watanabe, S.-i., and Team, H. P., "Hayabusa2 mission status: Landing, roving and cratering on asteroid Ryugu," *Acta Astronautica*, Vol. 171, 2020, pp. 42–54.

[4] Trisolini, M., Colombo, C., Tsuda, Y., et al., "Ejecta dynamics around asteroids in view of in-orbit particle collection missions," *72nd International Astronautical Congress (IAC 2021)*, 2021, pp. 1–10.

[5] Trisolini, M., Colombo, C., and Tsuda, Y., "Ejecta analysis for an asteroid impact event in the perturbed circular restricted three body problem," *31st JAXA Workshop on Astrodynamics and Flight Mechanics*, 2021.

[6] Arakawa, M., Saiki, T., Wada, K., Ogawa, K., Kadono, T., Shirai, K., Sawada, H., Ishibashi, K., Honda, R., Sakatani, N., et al., "An artificial impact on the asteroid (162173) Ryugu formed a crater in the gravity-dominated regime," *Science*, Vol. 368, No. 6486, 2020, pp. 67–71.

[7] Krivov, A. V., Sremčević, M., Spahn, F., Dikarev, V. V., and Kholshevnikov, K. V., "Impact-generated dust clouds around planetary satellites: spherically symmetric case," *Planetary and Space Science*, Vol. 51, No. 3, 2003, pp. 251–269.

[8] Sachse, M., Schmidt, J., Kempf, S., and Spahn, F., "Correlation between speed and size for ejecta from hypervelocity impacts," *Journal of Geophysical Research: Planets*, Vol. 120, No. 11, 2015, pp. 1847–1858.

[9] Yu, Y., Michel, P., Schwartz, S. R., Naidu, S. P., and Benner, L. A., "Ejecta cloud from the AIDA space project kinetic impact on the secondary of a binary asteroid: I. mechanical environment and dynamical model," *Icarus*, Vol. 282, 2017, pp. 313–325.

[10] Housen, K. R., and Holsapple, K. A., "Ejecta from impact craters," *Icarus*, Vol. 211, No. 1, 2011, pp. 856–875.

[11] Holsapple, K. A., and Housen, K. R., "A crater and its ejecta: An interpretation of Deep Impact," *Icarus*, Vol. 191, No. 2, 2007, pp. 586–597.

[12] Holsapple, K. A., and Housen, K. R., "Momentum transfer in asteroid impacts. I. Theory and scaling," *Icarus*, Vol. 221, No. 2, 2012, pp. 875–887.

[13] Richardson, J. E., Melosh, H. J., Lisse, C. M., and Carcich, B., "A ballistics analysis of the Deep Impact ejecta plume: Determining Comet Tempel 1's gravity, mass, and density," *Icarus*, Vol. 191, No. 2, 2007, pp. 176–209.

[14] Soldini, S., and Tsuda, Y., "Assessing the hazard posed by Ryugu ejecta dynamics on Hayabusa2 spacecraft," *26th International Symposium of Space Flight Dynamics*, 2017, pp. 1–11.

[15] Carry, B., "Density of asteroids," *Planetary and Space Science*, Vol. 73, No. 1, 2012, pp. 98–118.